Journal of Power Sources 196 (2011) 7126–7135

Contents lists available at ScienceDirect

Journal of Power Sources

journal homepage: www.elsevier.com/locate/jpowsour

Crack severity in relation to non-homogeneous Ni oxidation in anode-supported solid oxide fuel cells

J.L. Young, V.I. Birss*

Department of Chemistry, University of Calgary, 2500 University Drive NW, Calgary, Alberta T2N 1N4, Canada

ARTICLE INFO

Article history:
Received 27 July 2010
Received in revised form 1 September 2010
Accepted 2 September 2010
Available online 15 September 2010

Keywords:
Ni–YSZ anode
Ni oxidation
Redox cycling
Solid oxide fuel cell (SOFC)
Electrolyte cracking

ABSTRACT

The full oxidation of Ni–YSZ anode-supported cells at high temperatures (>700 °C) is shown here to lead to much more severe degradation (larger quantity and wider cracks in the electrolyte) than at lower temperatures. This correlates with the linear mass gain/time profile observed in TGA experiments at high temperatures, indicative of diffusion controlled Ni oxidation and thus the presence of O_2 (and Ni/NiO) concentration gradients into the depth of the anode layer. At low partial pressures of O_2, the severity of cracking also increases. SEM studies of partially oxidized anode layers confirmed that Ni oxidation is non-homogeneous when carried out at either high temperatures or low pO_2, in which case the outer regions of the anode (near the anode/air interface) become almost fully oxidized, while the inner regions (near the electrolyte) remain metallic. Under these conditions, the continued volume expansion associated with NiO formation can then only occur towards the electrolyte, increasing the compressive stress inside the anode as the Ni continues to be oxidized, leading to electrolyte cracking and warping (convex to the electrolyte). To prevent severe degradation to the cell, efforts should therefore be made to avoid gradients in NiO/Ni content during oxygen exposure of Ni–YSZ anode-supported cells at high temperatures.

1. Introduction

Solid oxide fuel cells (SOFCs) are devices that convert the chemical energy of a fuel (ranging from H_2 to reformed hydrocarbon fuels, such as gasified coal) to electricity and high grade waste heat with high efficiency and low pollution. Nickel–yttria stabilized zirconia (Ni–YSZ) cermets are in widespread use as SOFC anode materials due to their ease of fabrication, high porosity, chemical and physical stability in reducing environments, and very good electrocatalytic activity for hydrogen oxidation [1]. The use of Ni–YSZ anode-supported architectures [2,3] further improves manufacturability, as well as cell performance, due to a low overall cell ohmic resistance. This allows operation at low operating temperatures (<750 °C vs. 1000 °C), thus permitting the use of low cost materials for stack components and a wide variety of cathode materials, such as those that produce resistive interfaces during high temperature manufacturing [1].

However, one of the serious challenges experienced by Ni-based anode-supported cells (this is not a major problem for cathode or electrolyte supported cells [4]) is the inadvertent oxidation of Ni when air enters the hot anode chamber, such as during system malfunction or shutdown while the temperature of the cell is still high (600–1000 °C). The rapid formation [5] of NiO (reaction (1)) results in a large volume increase (~65%) with associated morphology changes, causing severe degradation of the cell.

$$Ni + ½O_2 \rightarrow NiO \quad (1)$$

NiO subsequently reduces to Ni upon returning to a normal (H_2) operating environment and therefore this sequence of events is commonly referred to as a "redox" cycle.

While it is known that the reduction of NiO will itself not damage the cell [6], the mechanical damage to the electrolyte after only a single oxidation event can cause severe performance loss [7]. A model of the redox cycling process has been expounded by Klemenso et al. [8], suggesting that, upon initial *in situ* reduction, the Ni particles reorganize by sintering mechanisms. Upon re-oxidation by exposure to air, it is not possible for the NiO network to return to its original distribution. It was also shown [9] that the NiO that is formed on re-oxidation has a higher porosity and thus a larger volume than the initial oxidized state. Due to a combination of some or all of these factors, localized tensile stresses as high as 1000 MPa [10] can be experienced by the YSZ component of the anode layer and the electrolyte, while the yield strength of 8YSZ (8 mole percent yttria) is only 300 MPa [11]. Further, it was demonstrated that,

* Corresponding author. Tel.: +1 403 220 6432; fax: +1 403 289 9488.
E-mail address: birss@ucalgary.ca (V.I. Birss).

0378-7753/$ – see front matter © 2010 Elsevier B.V. All rights reserved.
doi:10.1016/j.jpowsour.2010.09.002

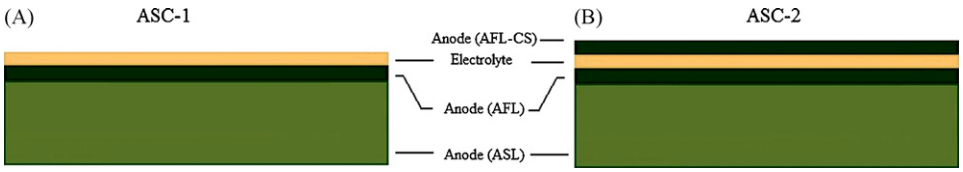

Fig. 1. Cells used for testing were (A) ASC-1 and (B) ASC-2.

if a cell experiences >0.1% strain [12,13], or 0.26% strain if the anode is <71% oxidized [14], then the YSZ electrolyte will crack. Investigations of cell performance by our group [4] and others [5,13,15] have confirmed that degradation after redox cycling of anode-supported SOFCs arises primarily from cracking in the anode layer. These studies have also shown that redox cycling does not appear to induce enough sintering to cause a loss of conductivity or triple phase boundary length. In fact, the interconnectivity of the Ni particles in the anode layer seems to be enhanced. However, this benefit is only temporary, as the Ni continues to re-sinter with time [16]. In cases where a loss of conductivity of the anode layer was seen with redox cycling, it has been suggested [16] that this is due to cracking of the YSZ component, allowing more Ni agglomeration than when no cracks are present.

In terms of crack prevention, Pihlatie et al. [13] showed that anodes with only 9% porosity exhibited 20 times more strain when subjected to redox cycling than those with 34% porosity. Recent work in our group [17] has shown that minimizing the extent of oxidation of the Ni particles in the region adjacent to the electrolyte is key to preventing cell degradation/failure. In this previous work [17], cells that were cooled at rapid ramp rates exhibited a lower Ni oxidation rate than at slower cooling rates, and it was found that, as long as the area adjacent to the electrolyte was <65% oxidized, the electrolyte would not crack. The entire anode in this case was 74% oxidized and thus a gradient in the degree of oxidation within the anode layer was observed (i.e., the rate of oxidation was not constant throughout the anode layer), helping to protect the electrolyte from cracking.

It was also noted in our earlier study [4] involving full redox cycles (100% of the Ni was oxidized and reduced) that the extent of degradation was less (fewer cracks and narrower crack widths) at lower oxidation temperatures. Ettler at al. [18] also found that warping after 50% oxidation of a 25 cm × 50 cm cell was much more severe at 800 °C than at 700 °C, attributing this to variable internal stresses within the anode. They also observed that the extent of Ni oxidation was not homogeneous in all directions within the anode layer due to O_2 transport limitations in the pores. Warping of cells during redox cycling may be caused by creep-related deformation (caused by high temperatures in the outer regions of the anode) [19], although uncertainty remains [20] regarding this explanation for cell degradation.

In the present work, it is shown that the quantity and severity of the cracks that form when a Ni–YSZ anode is fully oxidized both decrease as the oxidizing temperature decreases or as the pO_2 increases, the opposite conditions expected if thermal stress or creep were causing the damage. The extent of cracking is demonstrated here to be directly related to how significant the gradient in NiO content is into the depth of the anode layer, which, in turn, is related to how extensive the O_2 concentration gradients are within the anode and how homogeneous the oxidation rate was. When the outer regions of the anode layer are oxidized first, then NiO particles formed deeper in the anode layer can only grow inwards towards the electrolyte, causing increasing local compressive stresses and cracking. Therefore, severe degradation can be prevented by avoiding conditions that create non-homogeneous oxidation rates in the anode layer.

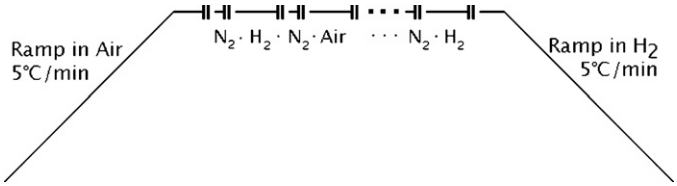

Fig. 2. Thermal and gas environment profile used for all Ni–YSZ anode redox experiments in the TGA.

2. Experimental methods

2.1. Cell/sample details

Two cell designs were used for the purposes of this study. The first (ASC-1, Fig. 1A) involved a 17 mm diameter disk, which was prepared by first tape casting a 1 mm thick anode-support layer (ASL), screen printing an anode functional layer (AFL) (10 μm), drying, screen printing a dense electrolyte layer (10 μm), drying and then co-firing at 1450 °C for 2 h. The second cell (ASC-2, Fig. 1B) employed a 13 mm dia disk that was prepared as per ASC-1, except that another AL (10 μm) was screen printed on the cathode (AFL-CS) side before drying and co-firing at 1450 °C for 2 h. Both the ASL and AFL of the ASC-1 and ASC-2 cells contained 57 mass% of NiO and 43 mass% YSZ, even though the ASL was fabricated with a 1 μm average particle size vs. 0.5 μm for the AFL. After fabrication, the ASL and AFL had a porosity of 22 and 14%, respectively, while after reduction, the ASL porosity was 38% and the AFL porosity was 30%.

2.2. Instrumentation

Redox cycling was carried out isothermally using a Setaram TAG 16 TGA/DSC dual chamber balance (600–900 °C). For reduction, 10% H_2–He was used, and for oxidation, the O_2 content was 0.1, 20 or 50%, with the balance being He. The samples used for this study were 80–250 mg pieces obtained by fracturing the intact (0.8–2 g) cell. Fractured specimens were placed (electrolyte down) in a shallow 100 μL Pt crucible or tested whole by suspending them above a 500 μL Pt crucible.

Samples were tested in the sequence outlined in Fig. 2, in which the samples were first heated to temperature in 0.1, 20 or 50% O_2 in He at 5 °C min^{-1}, followed by a N_2 purge for 10 min, and then switching to H_2 (10% H_2 in He). Reducing and oxidizing atmospheres were cycled, with intermittent 10 min N_2 purges for safety, using 3–12 h hold times in each reaction gas to ensure full reduction/oxidation of NiO/Ni, or for <20 min for partially oxidized samples. The samples were then cooled to room temperature at 5 °C min^{-1} for further analysis.

Cell imaging was carried out using a Nikon OPTIPHOT metallurgical microscope or a Philips FEI XL-30 environmental scanning electron microscope (SEM, 20 kV, 10 mm working distance) in vacuum mode to examine (gold-coated) the electrolyte, the ASL surface, and cell cross-sectional images before and after redox cycling. Cross-sections of the anode were prepared by fracturing samples that had been redox cycled and then mounting them on stubs. Some cross-sections were mounted in epoxy and polished

(320 and 600 grit emery paper and 0.01 μm alumina suspension) prior to examination.

3. Results and discussion

3.1. TGA study of Ni–YSZ anode oxidation during multiple redox cycles

The TGA oxidation profiles of newly manufactured 13 mm ASC-2 button cells that were isothermally oxidized and reduced at 700 and 800 °C in 5 successive full redox cycles are shown in Fig. 3A and B, respectively. The data have been normalized to the theoretical mass of oxygen (12.1%) in NiO in a fully oxidized NiO–YSZ anode. It should be noted that the apparently incomplete oxidation in Ox 1 after long times at all temperatures arises from the incomplete NiO reduction in the first reduction cycle (not shown, as summarized in Table 1). In fact, the anode is fully oxidized after the completion of each subsequent oxidation step in Fig. 3. Fig. 3 also shows that, as expected, it takes longer to completely oxidize the Ni–YSZ anodes at lower temperatures. Further, at 700 °C (Fig. 3A), it takes the same amount of time to oxidize 75% of the sample in all 5 cycles, while at 800 °C (Fig. 3B), the oxidation process becomes more rapid with each cycle until the fifth cycle, when the mass gain/time curves begin to overlap.

To explain the changes in the TGA mass/time profiles with cycling time, the Ni morphology was examined by SEM, as shown in Fig. 4 for the first and fifth full reduction steps at 700 °C (Fig. 4A and B, respectively) and at 800 °C (Fig. 4C and D, respectively). The atypically large agglomerates seen in Fig. 4 show that the Ni grains (within the agglomerates) have increased in size (from ~0.5 μm in

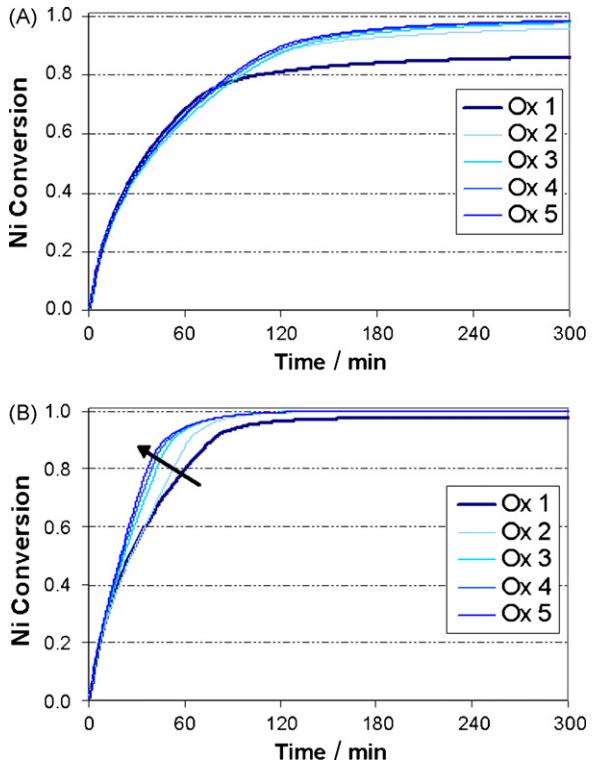

Fig. 3. Thermogravimetric analysis data in successive Ni–YSZ full oxidation steps during redox cycling of an ASC-2 cell (Fig. 2) at (A) 700 °C and (B) 800 °C.

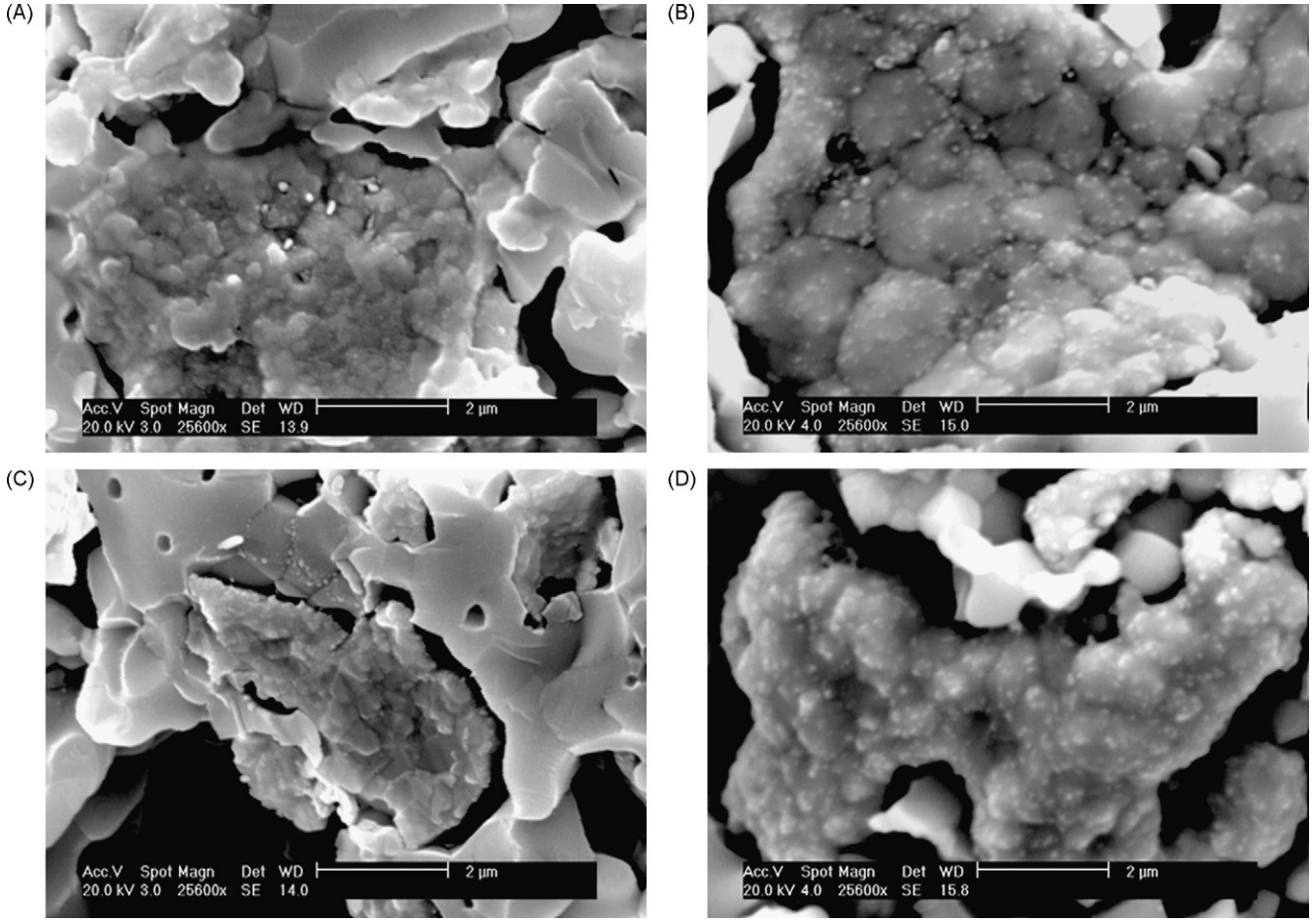

Fig. 4. SEM micrographs of Ni–YSZ in the anode-support layer of an ASC-2 cell in a fully reduced state after (A) first reduction at 700 °C, (B) 5 redox cycles at 700 °C, (C) first reduction at 800 °C, and (D) 5 redox cycles at 800 °C.

Table 1
Extent of NiO–YSZ reduction at various stages of TGA analysis (from Fig. 3).

Temperature (°C)	Completion of linear reduction region (%)[a]	Extent of NiO reduction (%) and time required[a]	Completion of linear reduction region (%)[b]	Extent of NiO reduction (%) and time required[b]
650	12	83 (10 h)	48	95 (10 h)
700	25	86 (10 h)	58	99 (10 h)
750	37	88 (8 h)	67	99.5 (6 h)
800	50	98 (4 h)	75	100 (4 h)

[a] In first redox cycle.
[b] In subsequent redox cycles.

Table 2
Cracking observed in ASC-2 cells after 5 redox cycles at various temperatures.

Temperature (°C)	Electrolyte cracks mm^{-1}[a] (from cross-section)	Cracks penetrating AFL[b] (ASC-2 cells only)	Parallel edge cracks (Fig. 11, 20% pO_2)
650	4.5	No	No
700	6.5	Yes	No
750	13.2	Yes	Yes
800	18.5	Yes	Yes

[a] Cracks mm^{-1} is the number of the cracks observed in the cross-section of the electrolyte, as viewed by SEM.
[b] The presence of cracks through the AFL is an indication of the severity of cracking.

the as-reduced sample to ~0.75 μm after redox cycling). Additionally, the Ni grains are more spheroidized and some nanocrystallites of Ni have appeared on the surface of the Ni agglomerates after redox cycling. At 700 °C, the grains are more coherent, due to slightly less sintering than at 800 °C, although the differences are not dramatic. Overall, the Ni morphology does not change significantly after 5 full redox cycles at 700 °C. Therefore, despite large changes in the oxidation rates with cycle number in Fig. 3, at least at 800 °C (Fig. 3B), changes in the Ni morphology likely do not contribute to the differences in the mass/time profiles. It will be

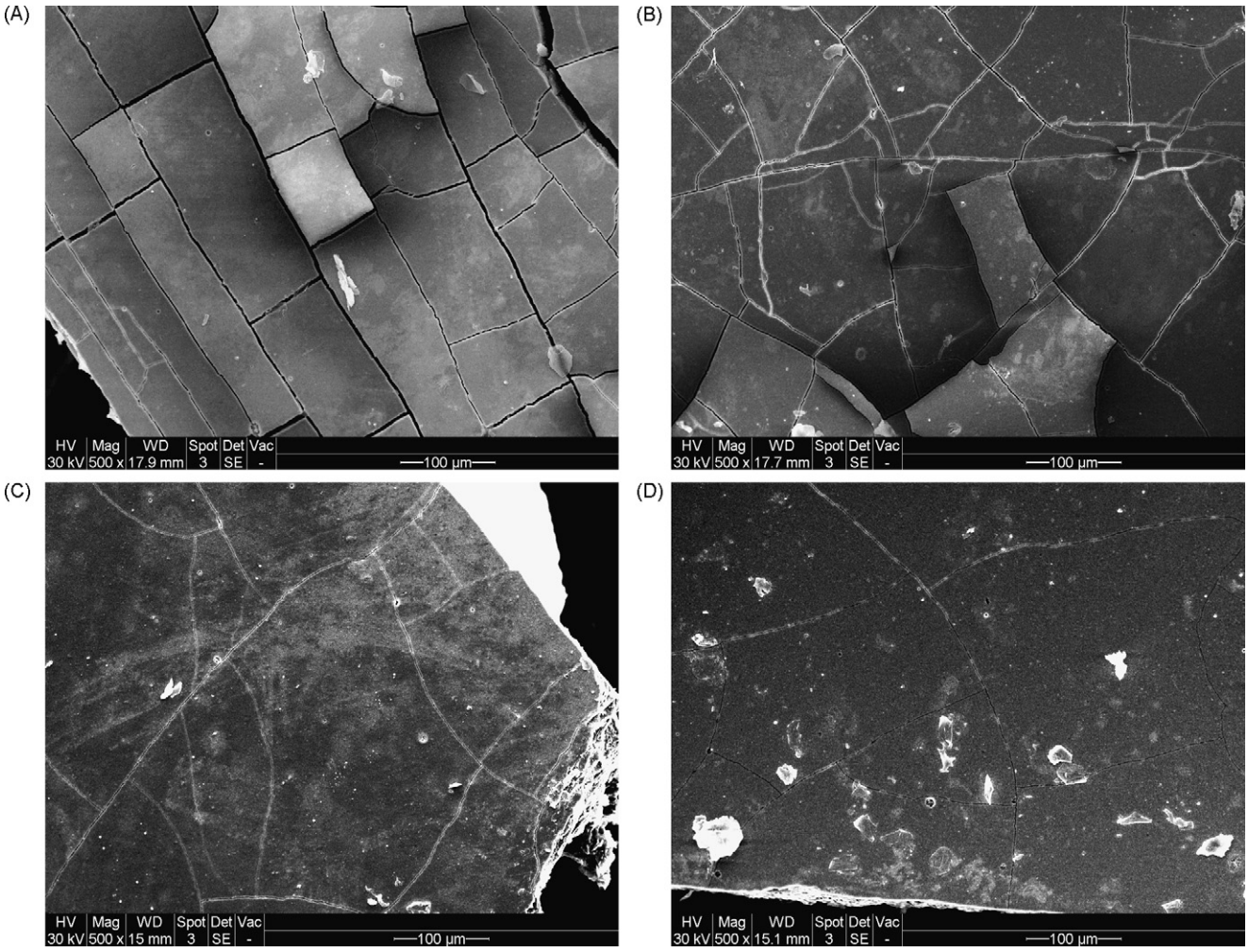

Fig. 5. SEM images of the electrolyte of an ASC-1 cell, showing the cracks that form after 2 full redox cycles at (A) 900 °C, (B) 800 °C, (C) 700 °C, and (D) 600 °C.

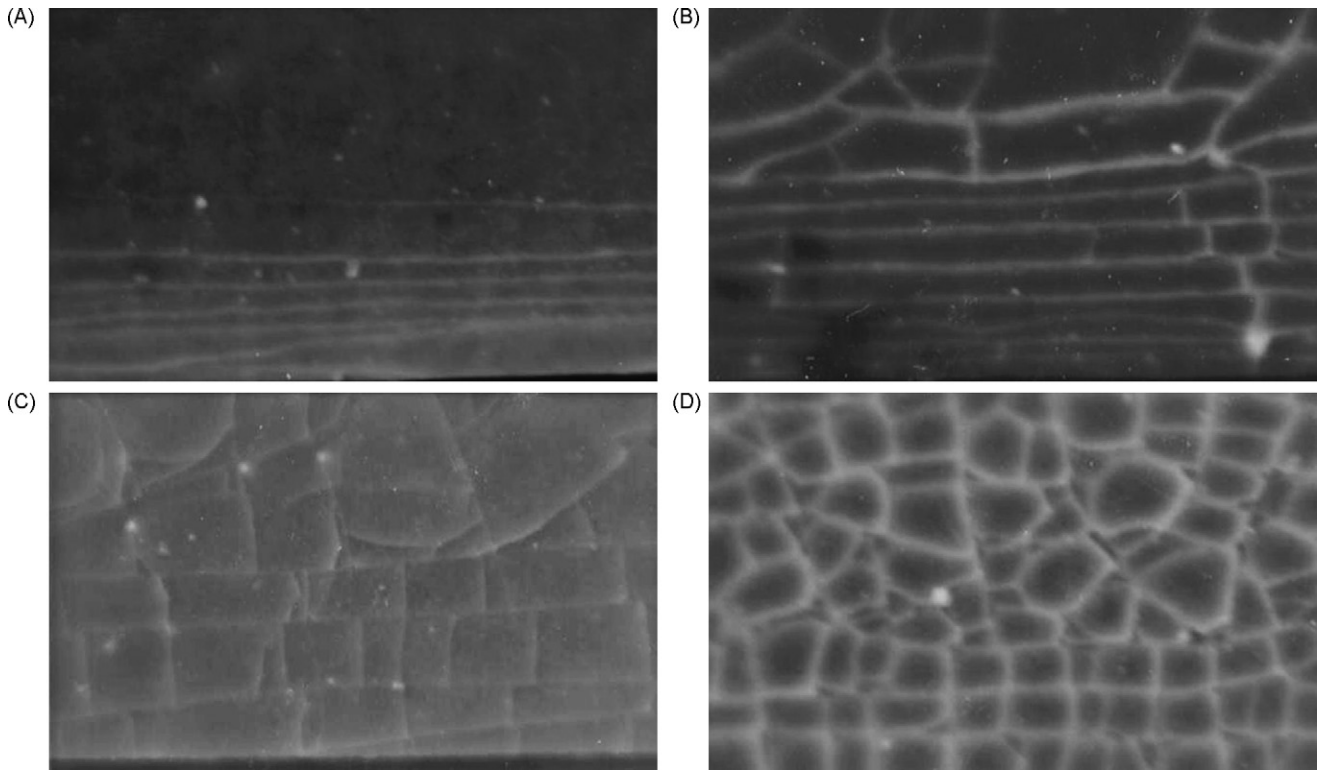

Fig. 6. Optical microscopy images (20× magnification) of electrolyte cracks after 5 redox cycles of an ASC-1 cell when the cell was partially oxidized at 800 °C to (A) 61%, (B) 73%, (C) 90% and (D) 100% of the total Ni in the anode layer.

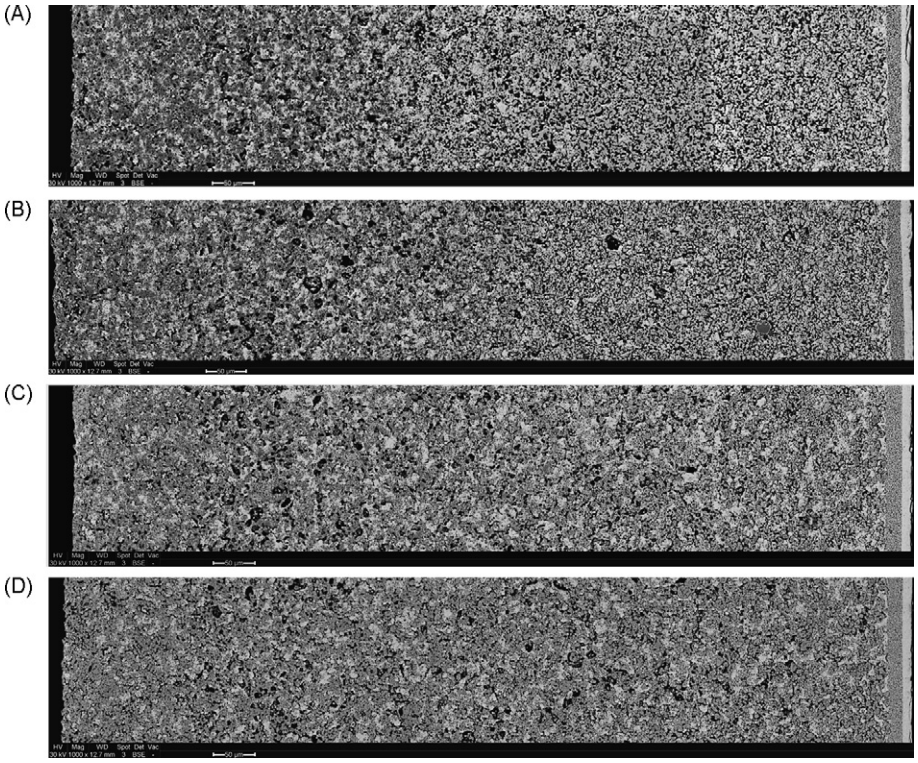

Fig. 7. Compilations of SEM BSE images of an ASC-1 cell partially oxidized (~50%) at (A) 900 °C, (B) 800 °C, (C) 700 °C and (D) 600 °C. NiO is dark grey, while Ni and YSZ are both white and thus indistinguishable. At high temperatures (>700 °C), NiO is the dominant phase near the anode/air interface (left), while adjacent to the electrolyte (right), Ni and YSZ are the major phases present. At lower temperatures (≤700 °C), NiO is much more evenly distributed throughout the anode layer cross-section. Gamma settings have been altered to enhance contrast between phases.

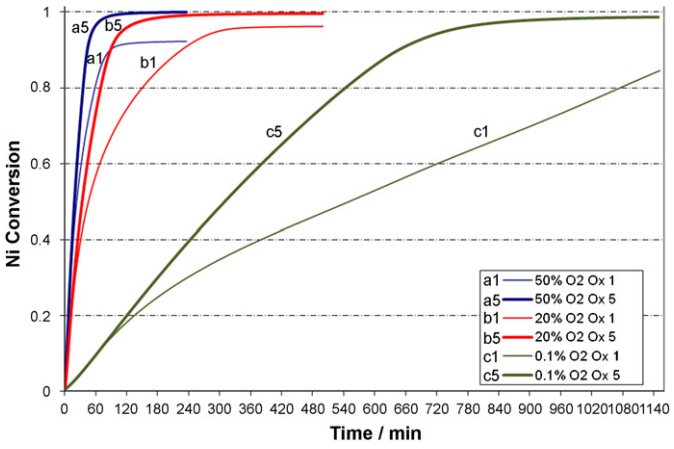

Fig. 8. Measured mass gain of Ni–YSZ anode at 800 °C in a fresh ASC-1 cell (Ox 1) and in the fifth oxidation cycle (Ox 5) during oxidation in (a) 50% O_2–He, (b) 20% O_2–He and (c) 0.1% O_2–He.

shown below that the increased Ni oxidation rate with multiple redox cycling is more likely due to O_2 penetration into the inner anode regions through cracks that develop in the YSZ electrolyte, especially at higher oxidation temperatures.

Fig. 3 also shows that, at 700 °C, the oxidation profile appears parabolic at all times, while at 800 °C, the profile is generally linear. The linearity seen in Fig. 3B, extending to 90% oxidation at 800 °C after the first cycle, implies that gas diffusion in the pores is rate limiting, i.e., that O_2 is reacting as rapidly with Ni as it enters the pores of the anode. Thus, a concentration gradient of O_2 through the depth of the anode is present, and this, in turn, implies that the anode layer contains a gradient of Ni and NiO, with more NiO in the outer regions of the anode and less deep inside the pores. The fact that this is more pronounced for anodes oxidized at 800 °C vs. 700 °C has been seen previously [18] and will prove to be important in the results shown in the following sections.

3.2. Effect of redox cycling temperature on fully and partially oxidized Ni–YSZ anodes

Optical microscopy and SEM analysis were used to establish the effect of the temperature at which Ni–YSZ anodes were both fully and partially oxidized on the resulting degree of crack damage. The exposed surface of the electrolyte layer of ASC-1 cells (Fig. 1A), the Ni–YSZ layer on the cathode side of ASC-2 cells (Fig. 1B), as well as cross-sections of both cell types, were examined to determine the extent and type of cracking observed (Table 1).

In the first set of experiments, all of the anodes were fully oxidized, but at different temperatures (600–900 °C). The impact of temperature was found to be quite extreme, as shown by SEM analysis in Fig. 5A–D after oxidation at 900–600 °C, respectively, and as also summarized in Table 2. Severe cracks were observed after full oxidation at >700 °C (Fig. 5A and B), while at temperatures below this (Fig. 5C and D), the degree of cracking of the electrolyte was much less extensive, similar to what has been reported previously [18].

In Fig. 5A and B, the ASC-1 cells subjected to 2 full redox cycles at 900 and 800 °C, respectively, also show "buckling" of the electrolyte surface, where it appears that entire electrolyte fragments have been pushed out from the electrolyte plane. The associated severe electrolyte cracking would likely then allow O_2 to access the anode through the electrolyte side of the cell during redox cycling. This may then be responsible for the increase in oxidation rates seen with successive redox cycles in the TGA experiments at 800 °C in Fig. 3B. In contrast, the much less severe cracking (lower quantity and narrower cracks) seen at 700 and 600 °C in Fig. 5C and D would not allow significant O_2 to pass through to the anode, consistent with the relatively non-changing TGA mass/time profile with repeated redox cycles at 700 °C in Fig. 3A.

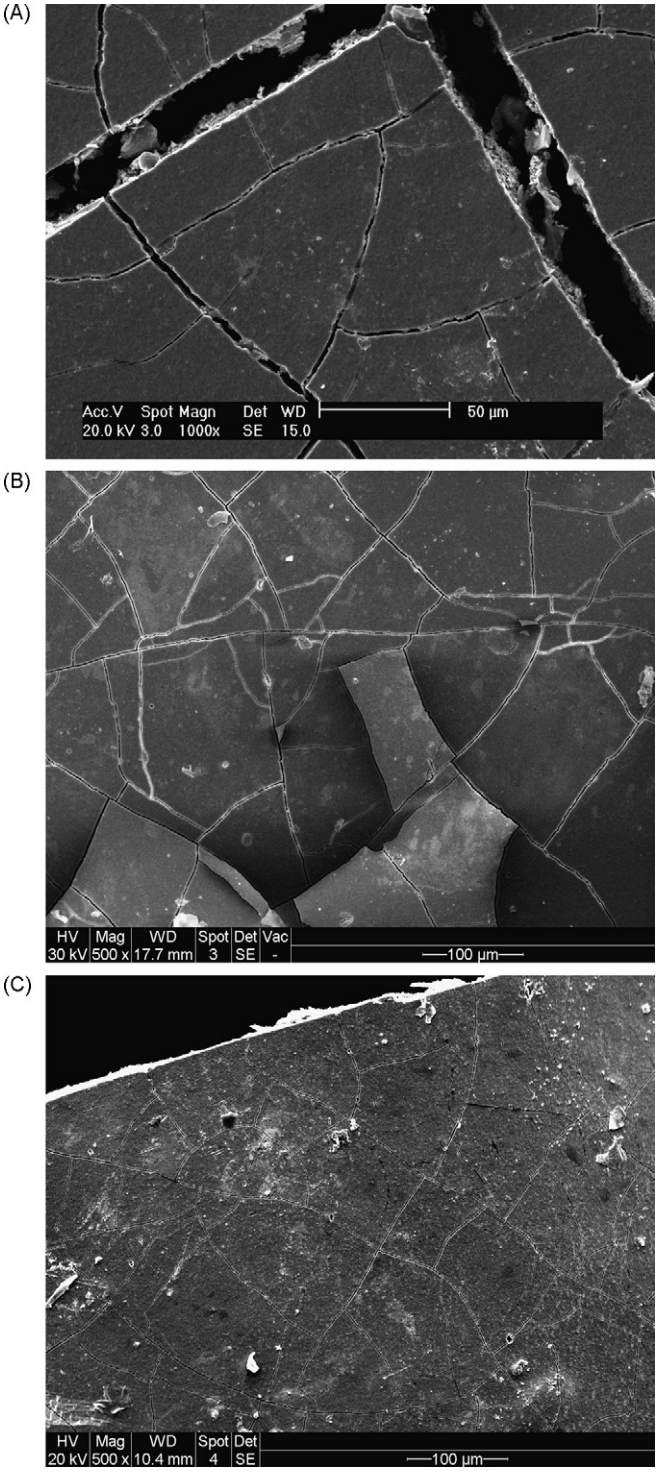

Fig. 9. SEM (secondary electron) images of the electrolyte of an ASC-1 cell after full oxidation at 800 °C in (A) 0.1% O_2–He, (B) 20% O_2–He and (C) 50% O_2–He.

To better understand the differences in cracking seen at different temperatures (Fig. 5), cells in which the anodes were only partially oxidized (≥50%) were also examined. At 800 °C (Fig. 6A), the first cracks to develop on the surface of the electrolyte after 61% of the Ni in an ASC-1 cell was oxidized at 800 °C were seen by

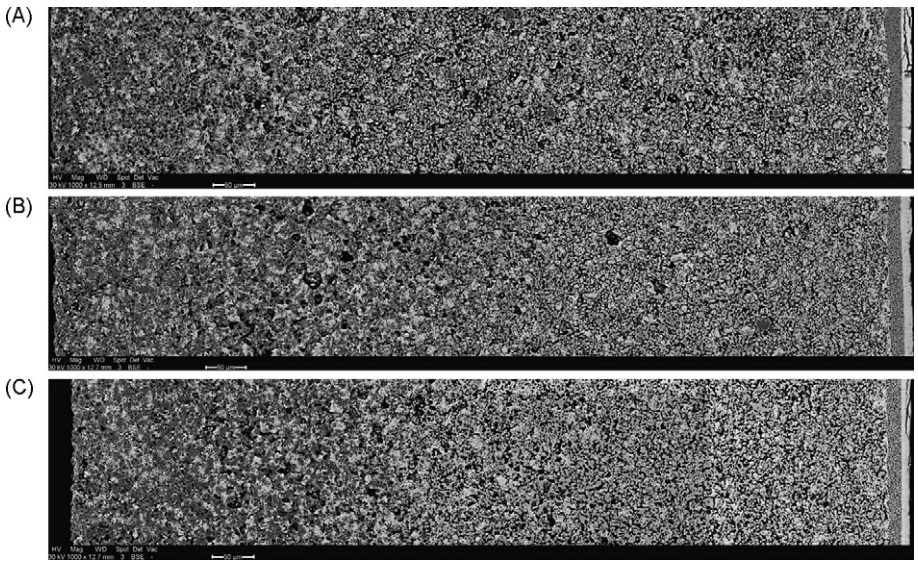

Fig. 10. SEM backscattered electron compilation images of the anode layer of an ASC-1 cell in which the Ni phase was ~50% oxidized at 800 °C in (A) 0.1% O_2–He, (B) 20% O_2–He and (C) 50% O_2–He, showing the non-isotropic distribution of NiO (dark grey) formation through the anode layer. Gamma settings have been altered to enhance contrast between phases.

optical microscopy to be near, and parallel to, the cell edges (where air is able to easily penetrate the porous anode region, especially adjacent to the electrolyte). With further oxidation (to 73%), cracks perpendicular to the cell edge develop, with some propagating to the middle of the cell, as shown in Fig. 6B. As the cell was oxidized still further, an increasing number of cracks propagated to the middle of the cell until a maximum was reached at ~90% oxidation (Fig. 6C), very similar to the 100% oxidized sample (Fig. 6D).

The development of cracks was seen to be very different at temperatures ≤700 °C, with no cracks seen parallel to the edges of the cell (as in Fig. 6A) and only cracks that randomly propagate across the electrolyte observed after oxidizing more than 80% of the Ni in the anode. Thus, there is a clear transition in the character of Ni oxidation between 700 and 750 °C, below which the parallel cracks do not occur and above which they do. This also correlates with the transition between minor and severe cracking (in terms of crack width and electrolyte buckling), as seen in Fig. 5.

Anode layers that were only 50% oxidized, but at different temperatures, were then closely examined by SEM analysis. Fig. 7A and B, involving samples that were oxidized to 50% NiO at 900 and 800 °C, respectively, show a compilation of backscattered electron (BSE) images along the entire thickness of the anode layer. These demonstrate that NiO (grey) is highly prevalent in the outer half of the anode layer, but that Ni (white, and indistinguishable from YSZ) is dominant in the inner (electrolyte side) half of the anode. In Fig. 7C, at 700 °C, however, this gradient in the NiO/Ni content is much less clear, and at 600 °C (Fig. 7D), Ni appears to be oxidized homogeneously throughout the entire anode-support layer.

Thus, these results show clearly that a gradient in the Ni/NiO composition of the anode layer (and hence in the Ni oxidation rate), seen here after partial oxidation at 800 °C, correlates with extensive electrolyte cracking for both partially and fully oxidized cells. The pronounced gradient in composition at 800 °C was also predicted by the linear TGA mass/time data at this temperature in Fig. 3B, indicative of mass transport controlled conditions (and related gradients in the O_2 concentration) during Ni oxidation.

3.3. Effect of variable pO_2 on electrolyte cracking due to redox cycling: further evidence for impact of graded NiO content

In order to test the hypothesis that a graded NiO content, formed in the porous Ni–YSZ anode layer during redox cycling, exacerbates the severity of cracking, and that thermal shock or high temperature creep [19] are not responsible for cracking, a variable pO_2 was used for redox cycling of fresh fragments of ASC-1 samples at 800 °C. Fig. 8 shows the TGA results obtained during the first and fifth oxidation steps at normal O_2 concentrations (~20% O_2–He), higher pO_2 (~50% O_2–He), and very low O_2 concentrations (~0.1% O_2–He). Based on the linear mass/time profile at low pO_2 (Fig. 8), it is clear that O_2 is reacting with Ni as quickly as it enters the pore structure. Analogous to the 800 °C data in Fig. 3, the low pO_2 data in Fig. 8 predict that extreme O_2 and NiO/Ni concentration gradients should be present and that cracking should be severe. In contrast, at 20 and 50% O_2, there is more evidence for parabolic mass/time behavior (Fig. 8), and thus less cracking damage would be expected.

Indeed, after 5 full redox cycles, the severity of the damage to the cell was found to be the most significant at the lowest pO_2. The cracks are large, deep and visible to the eye (Fig. 9A), as compared to the case in 20 and 50% O_2 (Fig. 9B and C, respectively). Cracks in the electrolyte parallel to the edge of the cell (similar to Fig. 6A) were noted. Additionally, at the lowest pO_2, the cell became warped (convex to the electrolyte) after 5 full redox cycles in the TGA. This result is very similar to what was observed by Stathis et al. [21], who oxidized a Ni–YSZ anode using only steam (at a low pO_2). The reaction rate was linear with time during oxidation in their case as well, corroborating that, at low pO_2, the reactant is quickly exhausted as it enters the porous anode layer, thus leading to significant internal concentration gradients. At 20 and 50% O_2, the degradation is much less severe than at low pO_2; at 50% O_2 (Fig. 9C), the cracks are the narrowest, and there are no parallel cracks seen on the electrolyte at the edges of the cell.

To further verify that the presence of gradients in the NiO and Ni content of the anode layers correlates with the severity of degradation observed, 50 ± 5% of the Ni in the anode was oxidized in a 0.1, 20 and 50% O_2 environment at 800 °C and then oxidation was stopped in each case. Fig. 10 shows the cross-sectional compilation images, demonstrating the presence of a significant gradient in the NiO and Ni content in the anode at the lowest O_2 concentration (Fig. 10A), but much less so after oxidation in 20% (Fig. 10B) and 50% O_2 (Fig. 10C).

Higher magnification SEM images of the outer region of the ASL (near the ASL/air interface) of each of the 50% oxidized anode are shown in Fig. 11, indicating that, at low pO_2 (Fig. 11A), the Ni particles in this region have been completely converted to NiO. In 20%

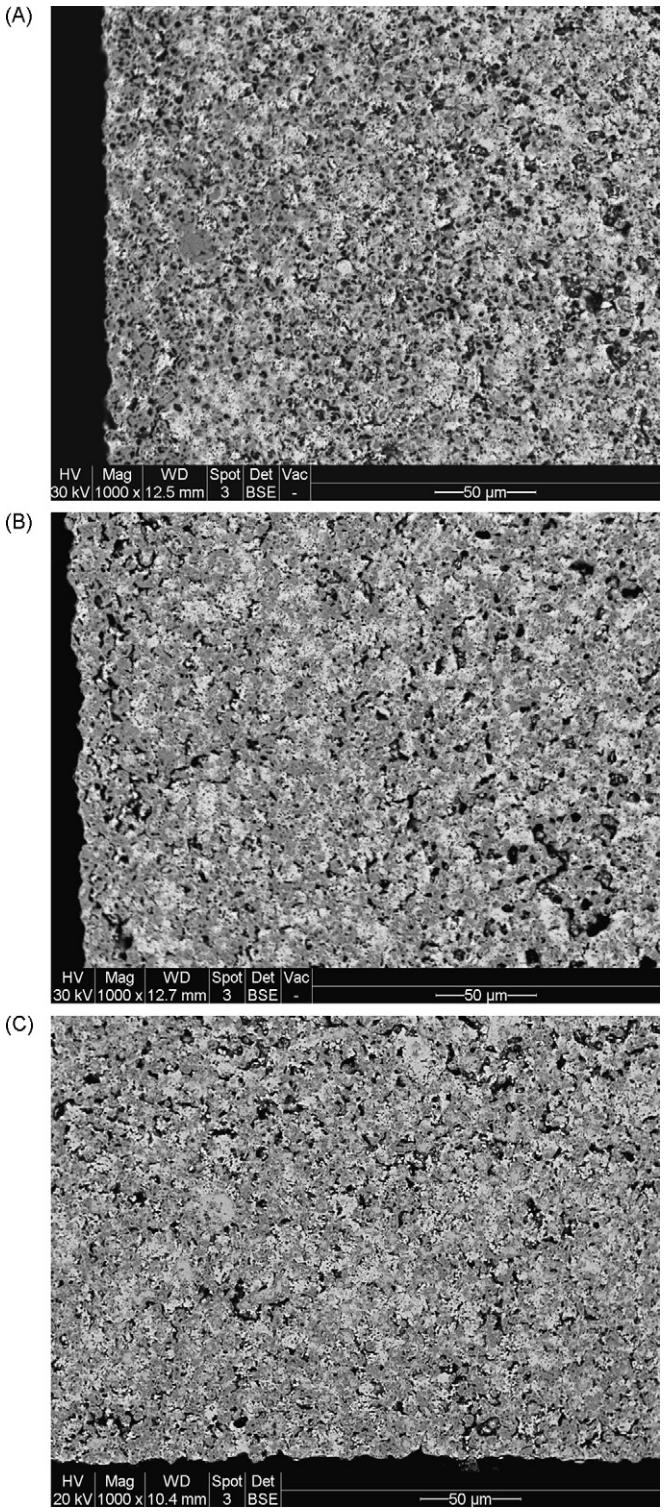

Fig. 11. SEM backscattered electron images of the ASL cross-section at the outer edge (ASL/air interface) after oxidation of 50% of the Ni in (A) 0.1% O_2–He, (B) 20% O_2–He and (C) 50% O_2–He. The lightest shade of grey is YSZ, the darkest shade of grey is NiO, and the intermediate shade of grey (primarily observed in C) is Ni, seen to be surrounded by a dark grey NiO coating. Gamma settings have been altered to enhance contrast between phases.

O_2 (Fig. 11B), Ni is seen in the core of some of the NiO particles, while at 50% O_2, Ni (surrounded by dark regions of NiO) is seen to be quite abundant in this region of the anode.

Overall, it is clear that lowering the pO_2 results in a significant gradient in the NiO content in the anode layer when the anode is partially oxidized, as was also the case when the temperature of oxidation was increased. For example, the NiO gradient (Fig. 7A) and the extent of electrolyte cracking (Fig. 5A) at 900 °C and 20% O_2 is comparable to what is seen after exposure of the anode to a low pO_2 at 800 °C. In both cases, the anode layers are highly oxidized in the outer regions of the anode (near the anode/air interface) and much less oxidized deeper in the anode, thus leading to similarly severe cracking. As was stated previously [18] and is confirmed here, the rate of permeation of air through the anode layer relative to the rate of Ni oxidation are the key factors determining whether Ni oxidation is isotropic or non-isotropic.

3.4. Model of enhanced degradation of Ni–YSZ anodes caused by non-isotropic oxidation during redox cycling

The TGA oxidation data (Fig. 3) demonstrated that the mass gain/time profile of anode-supported cells (Fig. 2) is essentially linear at 800 °C, but not at 700 °C, suggesting that Ni oxidation is diffusion controlled at high temperatures (>700 °C). This, in turn, implies that substantial O_2 concentration gradients, and hence NiO (and Ni) gradients, are present in the anode layer at the higher temperature conditions. In Section 2, these predictions were verified, with cross-sectional compilation images of partially oxidized anodes showing a distinct gradient in NiO content through the full thickness of the ASL at 800 °C that was not as prevalent for anodes oxidized at 700 °C. Importantly, anodes that were fully oxidized at higher temperature conditions showed significantly more severe electrolyte cracking (Fig. 5). In Section 3, it was shown that lowering of the pO_2 also leads to mass transport controlled Ni oxidation, along with significantly increased cell degradation, with cross-sectional images of partially oxidized anodes confirming the presence of a gradient in the Ni and NiO content through the full thickness of the ASL.

The conclusion reached from these results is that the presence of a gradient in NiO content during anode oxidation exacerbates damage due to cell cracking. A similar conclusion was also reached by Ettler et al. [18], who investigated the redox stability of a 25 cm × 50 cm cell under varying cell temperature, direction of gas flow, and gas flow rate conditions. The mechanism for the increased degradation in the presence of NiO gradients was suggested [18] to involve the development of a high compressive stress in the oxidized part of the anode, causing the cell to warp. This makes sense, as the direction of warp was concave to the electrolyte, while the present results, and those in other studies [21], show that warping is convex to the electrolyte surface.

Other explanations for the increased cracking severity when the Ni/NiO gradients are more pronounced include thermal shock (due to the rapid increase in local temperature) and thermal stress (due to thermal expansion of the hotter oxidizing region vs. the rest of the anode layer). Others have speculated that creep [19] is responsible for the damage caused by non-isotropic Ni oxidation during redox cycling, resulting from the increase in temperature during the exothermic Ni oxidation reaction. These mechanisms (thermal shock, thermal stress, and creep) all require a higher local temperature in the oxidizing regions of the anode. However, in the case of Ni oxidation at the lowest O_2 content studied here (0.1% O_2), the rate of oxidation is constant for the >14 h required to fully oxidize the anode (Fig. 8). Therefore, the temperature increase (above 800 °C) should be negligible and yet the degradation patterns are the same as what is seen at 900 °C (parallel cracks starting at the edge of the cell, then propagating across the electrolyte and into the anode layer). In fact, the degradation observed at low pO_2 is the most severe of all, with cell warping and electrolyte cracks easily detected visually (Fig. 9A). Thus, our results show that cell cracking results from stress build-up as a consequence of the presence of a NiO concentration gradient (high concentration near air/anode

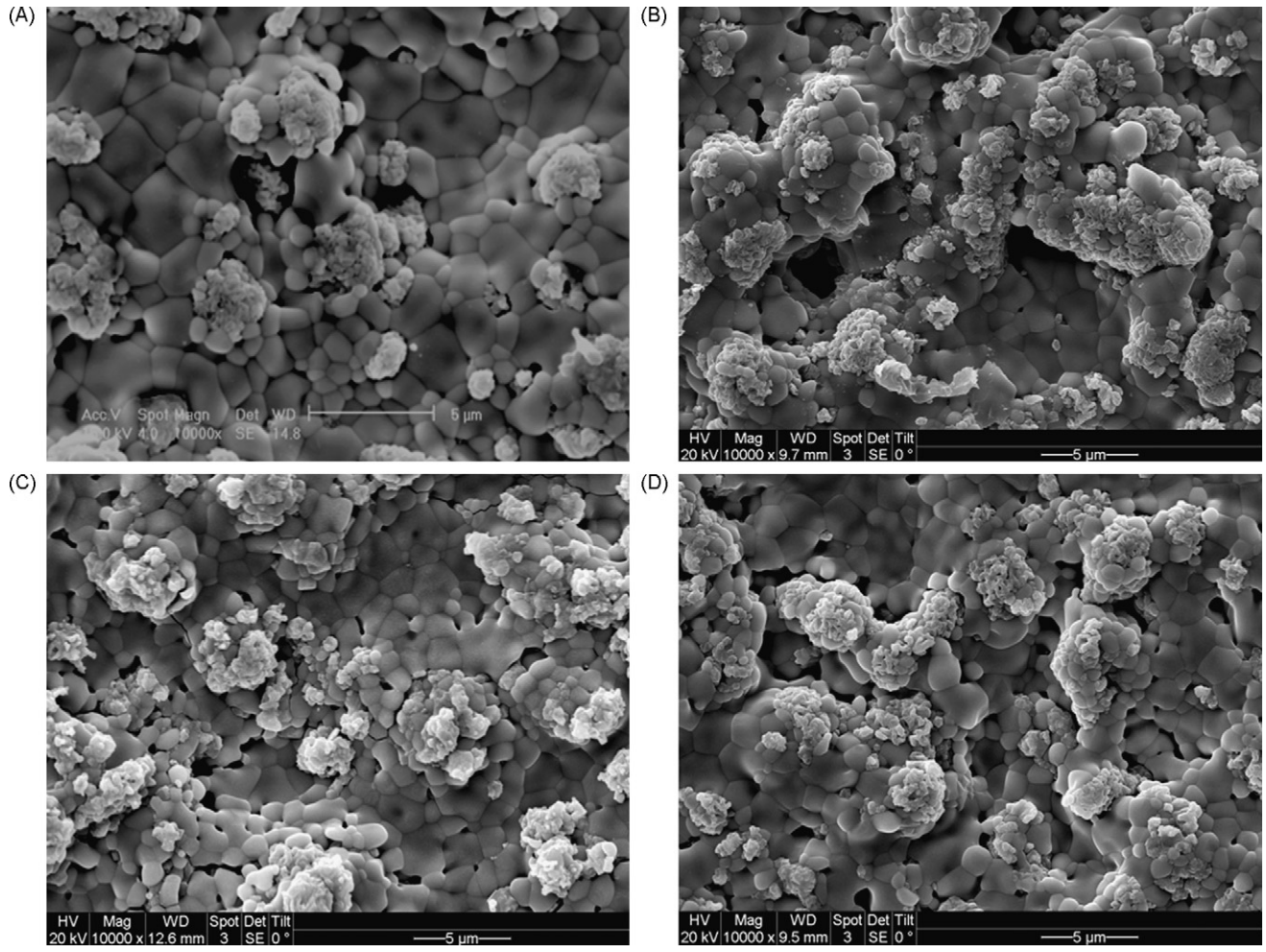

Fig. 12. SEM secondary electron images of the base of the ASL (ASL/air interface) after full oxidation (1 cycle) at 600 °C in (A) 20% O_2–He and (B) 50% O_2–He, and at 800 °C in (C) 20% O_2–He and (D) 50% O_2–He.

interface and low near the anode/electrolyte interface) in the anode layer, rather than from thermal effects.

We therefore propose the following model, which links the extent of cracking with the presence of gradients in the Ni/NiO content into the depth of the anode layer. Considering the extreme case when Ni in the outer region of the anode layer (near the anode/air interface at the anode base and at the edges of the cell (Fig. 6A)) becomes fully oxidized before O_2 penetrates further (e.g., at low pO_2 or at high temperatures), the outer region of the anode can relieve stress only by expanding into the most accessible pores deeper in the ASL. The NiO particles that form will then be rigidly fixed in place, since they will have filled the local pores. As the oxidation "front" proceeds deeper into the ASL with longer times of exposure to O_2, the newly formed NiO can only continue to grow in towards the electrolyte layer to reduce the stress. With increasingly fewer options available for Ni to NiO volume expansion as the oxidation front moves deeper, the stress increases in magnitude as the cell is oxidized further and, ultimately, can only be relieved by cracking the electrolyte. In extreme cases, the stress is very large and this leads to electrolyte warping and the propagation of cracks into the ASL.

Thus, it is suggested that, when the anode layer is homogeneously oxidized (no NiO concentration gradients present within the ASL, as during oxidation at high pO_2 and low temperatures), the stress that NiO formation causes within the anode layer is isotropic. Under these conditions, the expansion due to NiO growth will occur equally in all directions, resulting in NiO being ejected out of the anode layer at the ASL/air interface and into the anode layer's unoccupied pores. This, in turn, may prevent the formation of parallel cracks at the edges of the cell, since there would be a lower compressive force applying tension to the electrolyte.

SEM images of the anode/air interface should therefore provide an indication of how homogeneous Ni oxidation is through the anode layer. Fig. 12A and B shows that, as predicted, more NiO is ejected outwards at the ASL/air interface after oxidation in 50% O_2–He than at 20% O_2–He, respectively, both at 600 °C. To compare the effect of the Ni oxidation temperature, Fig. 12A and C shows that more NiO protrudes at the ASL/air interface at 600 than at 800 °C, respectively (both in 20% O_2), indicative of the less damaging and more homogeneous oxidation conditions within the ASL.

As the present experiments were carried out using a single anode-support layer morphology, the question arises as to how the cell cracking characteristics would be affected by a change in anode porosity. Ettler et al. [18] showed that, even when using a high porosity anode, the electrolyte continued to crack after a single redox cycle, although the quantity and characteristics of these cracks were not reported. In fact, it is expected that the effect of increased porosity would be similar to the impact of decreased operating temperature, since the gas transport to oxidation rate ratio will be diminished in both cases. Thus, parallel cracks should be less likely to occur and crack severity should be further reduced, all at constant temperature and pO_2.

For an operating SOFC stack, it has been speculated that air leakage may be quite slow during a redox event. Based on the present

work, this is the worst possible scenario, as these conditions would be expected to significantly increase the gradient in NiO content in the anode layer, in turn increasing the extent of degradation. To prevent severe degradation to the cell, it should therefore be cooled to a temperature that will minimize the Ni/NiO gradients, e.g., below 700 °C in atmospheric pO_2. As stated above, in a situation in which the outer regions of the anode are oxidized preferentially, and the inner regions remain metallic, a subsequent full oxidation of the remaining (inner) Ni particles will result in severe mechanical stress and damage to the electrolyte. This, however, will only prevent electrolyte cracking until more than ~80% of the Ni is oxidized. Thus, the temperature of the cell should be lowered to below 500 °C if the redox event is prolonged.

4. Summary

In this work, we show that non-homogeneous oxidization of Ni–YSZ anode-support layers, as results from oxygen exposure at high temperatures, enhances the severity of electrolyte cracking. This is consistent with the thermal gravimetric analysis data, which demonstrated that, at higher temperatures (>700 °C), the mass/time profiles are linear up to 90% oxidation at 800 °C after the first cycle. This indicates that gas diffusion in the pores is rate limiting, i.e., that O_2 is reacting as rapidly with Ni as it enters the pores of the anode. Under these conditions, a concentration gradient of O_2 is present into the depth of the anode layer and that the anode layer also contains a gradient of Ni and NiO, with more NiO in the outer regions of the anode and less deep inside the pores. At lower temperatures, the mass/time data are parabolic, indicative of the slow step in Ni oxidation being ion transport through the thickening NiO layer.

Optical microscopy and SEM analysis have confirmed that the extent of cracking of the cells is more severe when anodes are fully oxidized at higher temperatures, with entire electrolyte fragments pushed out from the electrolyte plane. Anodes that were only partially oxidized to ≥50% showed that, at 800 °C, the first cracks are near, and parallel to, the cell edges (allowing air to easily penetrate the porous anode region and enhance oxidation rates), while cracking is much less extensive at lower temperatures. SEM analysis confirms that, at high temperatures, NiO is highly prevalent in the outer regions of the anode layer, but that Ni is dominant closer to the electrolyte. At 700 °C, however, the NiO/Ni gradient is much less distinct and Ni is more homogeneously oxidized throughout the anode layer.

Lowering of the O_2 concentration (to 0.1% O_2) is also shown here to result in a significant gradient in the NiO content in the anode layer when the anode is partially oxidized, with the anode layer again being highly oxidized in the outer regions of the anode (near the anode/air interface) and much less oxidized deep inside the anode. This correlates with a linear mass gain in TGA experiments and very severe cracking and cell damage seen at these low pO_2 conditions. Importantly, as the rate of Ni oxidation at the lowest O_2 contents is constant for the many hours required to fully oxidize the anode, the local temperature increase should be negligible. This therefore rules out thermal shock, thermal stress, and creep as primary causes of cell cracking, which all require a higher local temperature in the oxidizing regions of the anode.

Thus, our results show that cell cracking results from stress build-up as a consequence of the presence of a NiO concentration gradient (high concentration near air/anode interface and lower near the anode/electrolyte interface) in the anode layer, rather than from thermal effects. The NiO formed in the outer regions of the anode will be rigidly fixed in place in the local pores, and therefore NiO that forms at longer times of oxidation can only grow inwards towards the electrolyte layer to reduce the stress. With increasingly fewer options available for Ni to NiO volume expansion as the oxidation front moves deeper, the stress is ultimately relieved by cracking of the electrolyte. Therefore, to prevent severe degradation due to cracking of the cell, efforts should be made to avoid gradients in the NiO/Ni content during oxygen exposure of Ni–YSZ anode-supported cells while at high temperatures.

Acknowledgements

We gratefully acknowledge the Natural Sciences and Engineering Research Council of Canada (NSERC) for support of this work through funding to the NSERC SOFC Canada Strategic Research Network. This work was also supported by an equipment and infrastructure grant from the Canadian Foundation for Innovation (CFI) and the Alberta Science and Research Authority. As well, we thank V. Vedasri and Dr. S. Paulson (both from the University of Calgary) for valuable discussions, and Drs. M. Schoel and T. Furstenhaupt (both at the University of Calgary) for assistance with the ESEM analyses.

References

[1] A. Atkinson, S. Barnett, R.J. Gorte, J.T.S. Irvine, A.J. McEvoy, M. Mogensen, S.C. Singhal, J. Vohs, Nature Materials 3 (2004) 17–27.
[2] M. Cassidy, K. Kendall, G. Lindsay, Proceedings fo the 1st European Solid Oxide Fuel Cell Forum, Lucerne, Switzerland, 1993, pp. 577–586.
[3] N.Q. Minh, R.A. Gibson, Proceedings fo the 1st European Solid Oxide Fuel Cell Forum, Lucerne, Switzerland, 1993, pp. 587–596.
[4] Young, J.L., Vedahara, V., Kung, S., Xia, S., Birss, V.I., 2007. ECS Transactions (ECST, vol. 7, issue 1). 10th International Symposium on Solid Oxide Fuel Cells (SOFC X), June 3–8, 2007, Nara, Japan.
[5] D. Fouquet, A.C. Muller, A. Webber, E. Ivers-Tiffée, Ionics 8 (2003) 103–108.
[6] H. Sumi, K. Ukai, M. Yokoyama, Y. Mizutani, Y. Doi, S. Machiya, Y. Akiniwa, K. Tanaka, Transactions of ASME 3 (2006) 68–74.
[7] M. Cassidy, G. Lindsay, K. Kendall, Journal of Power Sources 61 (1996) 189–192.
[8] T. Klemenso, C. Chung, P.H. Larson, M. Mogensen, Journal of the Electrochemical Society 152 (2005) A2186–A2192.
[9] J. Malzbender, E. Wessel, R.W. Steinbrech, Solid State Ionics 176 (2005) 2201–2203.
[10] J. Malzbender, E. Wessel, R.W. Steinbrech, Ceramic Engineering and Science Proceedings 25 (2004) 387–392.
[11] J. Kondoh, H. Shiota, K. Kawachi, T. Nakatani, Journal of Alloys and Compounds 365 (2004) 253–258.
[12] D. Sarataradis, A. Atkinson, Fuel Cells 7 (2007) 246–258.
[13] M. Pihlatie, T. Ramos, A. Kaiser, Journal of Power Sources 193 (2009) 322–330.
[14] J. Laurencin, G. Delette, B. Morel, F. Lefebvre-Joud, M. Dupeux, Journal of Power Sources 192 (2009) 344–352.
[15] J. Kong, K. Sun, D. Zhou, N. Zhang, J. Qiao, Rare Metals 25 (2006) 300–304.
[16] K. Klemenso, M. Mogensen, Journal of the American Ceramic Society 90 (2007) 3582–3588.
[17] V. Vedasri, J.L. Young, V.I. Birss, Journal of Power Sources 195 (2010) 5534–5542.
[18] M. Ettler, G. Blass, N.H. Menzler, Fuel cells 7 (2007) 349–355.
[19] A. Faes, A. Nakajo, A. Hessler-Wyser, D. Dubois, A. Brisse, S. Modena, J. Van Herle, Journal of Power Sources 193 (2009) 55–64.
[20] A. Morales-Rodriguez, A. Bravo-leon, G. Richter, M. Ruhle, A. Dominguez-Rodriguez, M. Jimenez-Melendo, Scripta Materiala 54 (2006) 2087–2090.
[21] G. Stathis, D. Simwonis, F. Tietz, A. Moropoulou, A. Naoumides, Journal of Materials Research 17 (2002) 951–958.